

Perturbative Treatment of Diffractive Dissociation at High Energies*

William R. Frazer[†]

Department of Physics, University of California, San Diego, La Jolla, California 92037

Dale R. Snider

Department of Physics, University of Wisconsin, Milwaukee, Wisconsin 53201

Chung-I Tan

Department of Physics, Brown University, Providence, Rhode Island 02919

(Received 18 June 1973)

Two-component models have been quite successful in fitting multiplicity distributions in high-energy hadronic collisions. The fact that the diffractive component is considerably smaller than the short-range-correlation component suggests the possibility of a perturbative expansion of the high-energy total cross section. We develop such an expansion in this paper, and examine some of its consequences. Prominent among these consequences are: (i) diffraction dissociation into high masses rises approximately logarithmically with energy at NAL-ISR (CERN Intersecting Storage Rings) energies, (ii) the short-range-correlation part of the cross section has high-energy behavior dominated by a "bare" Pomeron Regge pole, and (iii) the average multiplicity of particles produced in diffractive dissociation rises logarithmically with energy.

I. INTRODUCTION

Two-component models have been quite successful in accounting for the observed properties of high-energy multiparticle production.¹⁻³ The largest component, accounting for about 80% of the production, is characterized by short-range correlations (SRC) in rapidity space. The other 20% is diffractive; that is, characterized by constant partial cross sections and by the presence of large rapidity gaps. In this paper we shall explore the possibility of understanding the two components in the framework of a perturbative approach in which the SRC term is the zeroth approximation. Elastic scattering and low-mass diffractive dissociation are next in importance, followed by diffractive dissociation into high-mass states.

Diffractive dissociation into high-mass states is proportional to the triple-Pomeron coupling, which is known to be small.⁴⁻⁷ Nevertheless, it may be an important contribution to the total cross section at ISR (CERN Intersecting Storage Rings) energies, because it rises over a considerable energy range like the logarithm of the energy.^{8,9} We consider this contribution in detail in Sec. III, and show that the logarithmic rise is expected quite generally, regardless of details such as whether or not the triple-Pomeron coupling vanishes at $t=0$. At NAL-ISR energies its strength is determined not by the small dimensionless parameter η_P introduced by Abarbanel *et al.*,⁷ which is proportional to $g_{PPP}^2(0)$, but by an integrated parameter $\bar{\eta}_P$, which is proportional to $\int dt g_{PPP}^2(t)$. Higher-order terms in the perturbation expansion

are considered in Sec. IV, and all the terms with zero, one, or two large rapidity gaps are cataloged in Fig. 8.

The analysis of the cross section according to the number of rapidity gaps,¹⁰ coupled with the inference from experiment that the term with no large gaps dominates, suggests the utility of introducing the concept of a "bare Pomeron." The bare Pomeron is built up out of the SRC portion of the cross section, and controls its asymptotic behavior,

$$\sigma_{\text{SRC}} \sim s^{\alpha_0(0)-1}. \quad (1.1)$$

Evidently $\alpha_0(0)$ is not very much less than unity, because the SRC part dominates the cross section, which is approximately constant. Moreover, the bare Pomeron is purely a simple pole in the J plane.

The diffractive terms, with at least one large rapidity gap, have asymptotic behavior characterized by a branch point near $J=1$, in addition to the bare Pomeron pole. The way in which these J -plane singularities combine to form the physical Pomeron (the J -plane singularity of σ_T at or near $J=1$) cannot be determined without summing all terms of our perturbation expansion. We therefore consider in Sec. V a simple model in which the series can be summed. The model, which is a variation of the Chew-Snider model,¹¹ shows that the bare Pomeron pole does not occur in the complete total cross section, but is instead replaced by a high-lying singularity which is "renormalized" in position and residue from the bare Pomeron.

To summarize, we construct in this paper a

perturbative expansion of high-energy total cross sections in powers of the triple-Pomeron coupling. The expansion will be useful at NAL-ISR energies, where only a few terms will provide a good approximation. As examples of problems to which this expansion is applicable, we discuss rising total cross sections, multiplicity distributions in diffractive dissociation, and (in a simple model) the relation between bare and physical Pomerons.

II. ZERO-ORDER TERMS

A. Short-Range-Correlation Component

It is becoming increasingly well established that correlations among particles produced at very high energies are predominantly of short range. The most direct evidence for SRC comes from recent measurements at the ISR of two-particle correlation functions.¹² Less directly, many phenomenological studies of the energy dependence of topological cross sections have arrived at the same conclusion: Between 80% and 100% of the inelastic production can be accounted for by an SRC mechanism, which we shall indicate graphically by the symbol in Fig. 1(a).

Short-range correlations were expected theoretically from several viewpoints. As pointed out by Wilson,¹³ and later but independently by DeTar,¹⁴ the SRC property of multiperipheral models underlies all their characteristic predictions. In recent years it has proven useful, both for conceptual and pedagogical reasons, to abstract the SRC property and use it to understand multiparticle phenomena without reference to specific models. Much additional insight and predictive power resulted from Mueller's analysis of inclusive reactions.¹⁵ In Mueller's analysis it became clear that the SRC property follows simply and directly if the highest-lying J -plane singularity is a simple, factorizable pole. Therefore we assume that the SRC component of the cross section for a - b scattering has the asymptotic behavior

$$\sigma_{ab}^{\text{SRC}}(s) \sim \beta_{aa0}(0)\beta_{bb0}(0)s^{\alpha_0-1}. \quad (2.1)$$

We shall call α_0 the "bare Pomeron" intercept. The numbers in Table I indicate $\alpha_0 \lesssim 1$.

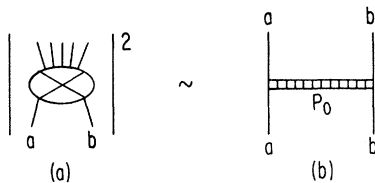


FIG. 1. Process with no large rapidity gaps (SRC cross section), whose leading singularity is the bare Pomeron P_0 .

Since it is well known that the idea of a simple-pole Pomeron singularity at $J=1$ is fraught with theoretical difficulties,¹⁶ we should emphasize at this point that we are inferring that the SRC component of the cross section, not the total cross section itself, has asymptotic behavior controlled by the bare Pomeron α_0 . In Sec. V we shall show in the context of a soluble model that the total cross section does not have a pole at $J = \alpha_0$.

While we shall not have need of a detailed model of SRC production in this paper, nor shall we attempt to construct a realistic model, there is a second property of the SRC component which we infer from the data and which will be essential in defining our perturbation approach: The SRC component involves no Pomeron exchange, and therefore (with high probability) gives rise to no large gaps in the rapidity distributions of individual events. One way to see this is to start from the Mueller generating function expansion,¹⁷

$$\sum_{n=0}^{\infty} \frac{\sigma_n(s)}{\sigma} z^n = \exp \sum_{n=1}^{\infty} \frac{f_n(s)}{n!} (z-1)^n, \quad (2.2)$$

where the σ_n 's are the partial cross sections for the production of n particles. If all correlations are short-range, the multiplicity moments f_n behave as follows:

$$f_n \sim a_n \ln s + b_n. \quad (2.3)$$

Differentiating Eq. (2.2), one then finds for the partial cross sections

$$\sigma_n(s) \sim \sigma(s) P_n(\ln s) s^{-\delta}, \quad (2.4)$$

where P_n denotes a polynomial of degree n , and where $\delta = -\sum_{n=1}^{\infty} (-1)^n a_n / n!$. Equation (2.4) shows the behavior characteristic of multiperipheral models, in which all partial cross sections show the same power behavior. Low-multiplicity cross sections are observed experimentally to fall with increasing energy; the fits in Refs. 1-3 yield $\delta \approx 0.8$ to 1.0 . Hence all partial cross sections arising from the SRC component fall like $s^{-\delta}$,

TABLE I. Values of SRC and diffractive cross sections in p - p scattering, according to fits described in Ref. 1. Superscript n on σ_D^n indicates number of negative particles produced. Since these numbers are obtained using a specific model, no reliable estimate of their accuracy is possible.

E_L (GeV)	σ_{SRC} (mb)	σ_D^0 (mb)	σ_D^1 (mb)	σ_D^2 (mb)	σ_D^3 (mb)	σ_D (mb)	$\langle n_D \rangle$
50		No satisfactory fit					
70	28.7	1.5	1.2	0.1	...	2.8	0.5
100	27.9	2.1	2.3	0.5	...	4.9	0.7
200	25.7	2.6	2.6	1.9	0.1	7.2	0.9
300	25.6	1.3	3.0	2.0	0.4	6.7	1.5

which implies (in a multiperipheral picture) the absence of Pomeron exchange and a consequent improbability of large rapidity gaps. This identification of the SRC component with events lacking large rapidity gaps has been inferred theoretically, but it will be interesting to subject it to experimental test.

In multi-Regge models the power δ in Eq. (2.4) is associated with the intercept of the Reggeon exchanged,⁴

$$\alpha_R(0) = 1 - \frac{1}{2}\delta. \tag{2.5}$$

The numbers quoted above from phenomenological fits give $\alpha_R(0) \approx 0.5-0.6$, which coincides with the location of the known prominent secondary trajectories.

In the preceding discussion we have not given a precise definition of the SRC component, but we have tacitly assumed that the extraction of the SRC component could be made by one of the two-component analyses of multiplicity distributions. All existing analyses rely, however, on detailed models of the components. Although it is encouraging that these detailed models agree rather well on the magnitudes of the two components, none of them are attractive as basic definitions. It is therefore more satisfying if we reverse the logic of our presentation and make the absence of large rapidity gaps the defining characteristic.

Following Chew,¹⁰ we decompose the total cross section according to the number of large rapidity gaps (larger than a specified Δ) observed in a given event. For example, Fig. 2 shows a three-gap event, provided that $x_2, x_4,$ and x_5 are greater than Δ . The total cross section can then be decomposed unambiguously according to the number of large gaps:

$$\sigma_{ab}(s) = \sigma_{ab}^{0,\Delta}(s) + \sigma_{ab}^{1,\Delta}(s) + \dots \tag{2.6}$$

This decomposition has the advantage of being well defined in terms of experimentally measurable quantities.

In the Appendix we analyze the relation between $\sigma_{ab}^{0,\Delta}$ and σ_{ab}^{SRC} in a simple model. We arrive at the following conclusions in the model, which we conjecture to be true in general: (i) The high-lying J -plane singularities of $\sigma_{ab}^{0,\Delta}$ are Regge poles (no

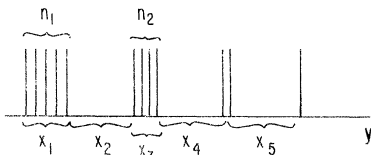


FIG. 2. Example of distribution of particles in rapidity space in a single event. Particle rapidities are marked by vertical lines.

cuts). Asymptotically,

$$\sigma_{ab}^{0,\Delta}(s) \sim s^{\alpha_0(\Delta)-1}, \tag{2.7}$$

where $\alpha_0(\Delta) < 1$.¹⁸ The leading pole position $\alpha_0(\Delta)$ (the bare Pomeron) depends on Δ , but for a range

$$\langle \Delta \rangle \ll \Delta \ll Y \tag{2.8}$$

(where $\langle \Delta \rangle$ is the average spacing in rapidity, and where Y is the available length of phase space in rapidity), the pole position $\alpha_0(\Delta)$ is almost independent of Δ . (ii) Long-range correlations are strongly suppressed in $\sigma_{ab}^{0,\Delta}$. Conversely, events with at least one large rapidity gap will show strong long-range effects. Therefore, to a good approximation, $\sigma_{ab}^{0,\Delta} \approx \sigma_{ab}^{SRC}$, where σ_{ab}^{SRC} is the quantity determined in multiplicity analyses.

The above conjectures are subject to experimental investigation. A reasonable choice of Δ suggested by Eq. (2.8) is $\Delta \approx 2-3$. When making numerical estimates in this paper, we shall choose Δ such that $e^\Delta = 10$.

B. Elastic and Quasielastic Cross Sections

The elastic cross section, with a value of about 7 mb through the Serpukhov-NAL energy range, is the second-largest component of the total cross section. In our expansion scheme it is zeroth-order in the triple-Pomeron coupling, but first-order in the number of large rapidity gaps. The lowest-order contribution to the total elastic cross section is found by replacing the Pomeron in Fig. 3 by the bare Pomeron, which results in the formula

$$\sigma_{el}^{(0)} \approx \frac{1}{16\pi} \int dt \beta_{aa0}^2(t) \beta_{bb0}^2(t) |\xi_0(t)|^2 s^{2\alpha_0(t)-2}, \tag{2.9}$$

where all quantities are the same as in Eq. (2.1), and $\xi_0(t)$ denotes the signature factor of the bare Pomeron. The couplings β_{aa0} are bare-Pomeron couplings, which are renormalized by higher-order effects into the coupling β_{aaP} to the complete-Pomeron singularity. We cannot calculate the relation between these couplings except in simplified

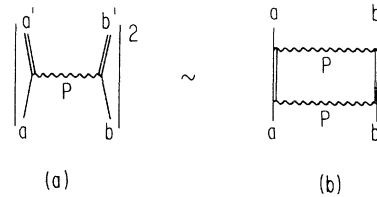


FIG. 3. Process with one large rapidity gap, with no large-mass clusters produced: includes elastic scattering as well as single and double diffractive dissociation to low masses. Double line indicates sum of all low-mass contributions.

models, such as the one presented in Sec. V.

The J -plane singularity of Eq. (2.9) is the usual AFS (Amati-Fubini-Stanghellini) cut, which results in a total elastic cross section falling with energy like $(a+b \ln s)^{-1}$, which is a reasonable first approximation to the observed behavior of the elastic cross section up to NAL energies.

At this point the question of self-consistency must be faced. If one approximates the Pomeron by the bare Pomeron in the calculation of σ_{el} , as we have done in Eq. (2.9), the resulting singularity governing the asymptotic behavior of $\sigma_T \approx \sigma_{SRC} + \sigma_{el}$ is the bare Pomeron plus the AFS cut. There are two ways to regard this inconsistency:

(i) *Perturbative approach.* One can regard Eq. (2.9) as a zeroth-order calculation of σ_{el} , which then defines a first-order Pomeron through $\sigma_T^{(1)} = \sigma_{SRC} + \sigma_{el}^{(1)}$. One can iterate to obtain higher-order terms. One difficulty with this approach is that the effective expansion parameter is the ratio of elastic to SRC cross sections, which is only $\approx \frac{1}{4}$. Even if one could sum these iterations [see (ii) below], the result would be correct only to zeroth order in the triple-Pomeron coupling.

(ii) *Self-consistent approach.* One can attempt to obtain self-consistency between the input Pomerons in Eq. (2.9) and the output Pomeron in σ_T . Many calculations of this type have been attempted, but all involve either unrealistic models or computer calculations.¹⁹ Nevertheless, it might be interesting to return to this problem in the present perturbative framework, trying for self-consistency only to zeroth order in the triple-Pomeron coupling and including terms with only one large rapidity gap. We shall not attempt such a calculation in this paper, but will rely on experiment for information about the Pomeron. Accordingly, we replace the bare Pomeron quantities in Eq. (2.9) by physical couplings and trajectory:

$$\sigma_{el} \approx \frac{1}{16\pi} \int dt \beta_{aa^*P}^2(t) \beta_{bb^*P}^2(t) |\xi_P(t)|^2 s^{2\alpha_P(t)-2}, \quad (2.10)$$

where $\alpha_P(t)$ is an effective Pomeron pole. It is an assumption, motivated by the success of factorization and short-range correlations, that the Pom-

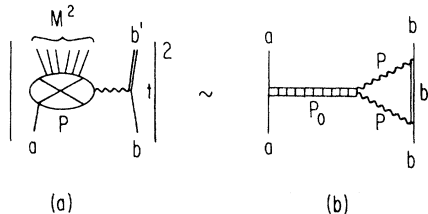


FIG. 4. Process with one large rapidity gap, leading to one large- and one small-mass cluster.

eron can be so represented to a good approximation.

The quasielastic cross sections, which are also of zeroth order in the triple-Pomeron coupling and have one large rapidity gap, are given by Eq. (2.10), but with couplings β_{aa^*P} or β_{bb^*P} , or both. When these contributions are added to the elastic cross section, one obtains what we shall call the total cross section for diffractive dissociation into low-mass states, $\sigma_{D,M < M_0}$, given by (see Fig. 3)

$$\sigma_{D,M < M_0}(s) \approx \frac{1}{16\pi} \int dt \left[\sum_{a^*} \beta_{aa^*P}^2(t) \right] \left[\sum_{b^*} \beta_{bb^*P}^2(t) \right] \times |\xi_P(t)|^2 s^{2\alpha_P(t)-2}, \quad (2.11)$$

where the sum includes $a^* = a$ and $b^* = b$, the elastic and quasielastic terms. The magnitude of this cross section is not yet well known at high energies. A rough estimate, which is probably a lower bound, can be obtained by adding the known cross sections for diffractive N^* production at 15 GeV/c; the sum is about 1.8 mb.²⁰ On the other hand, the Rochester-Michigan missing-mass experiment at 102 GeV finds the cross section for single diffractive dissociation into masses $M < 5$ GeV (excluding elastic) to be 6.8 mb, but a different background subtraction could cut this number in half.²¹ Other estimates, based on fits to multiplicity data, do not distinguish between high- and low-mass diffractive dissociation, but find the total diffractive component (excluding elastic) to be 5–7 mb.¹⁻³ Thus we have, at present, rough bounds on the total cross section for diffractive dissociation into low-mass states (including elastic), $9 < \sigma_{D,M < M_0} < 14$ mb.

III. FIRST-ORDER TERM: SINGLE DIFFRACTIVE DISSOCIATION INTO HIGH MASSES

A. Contribution to Total Cross Section

The term which is first-order in the triple-Pomeron coupling and which contains one large rapidity gap contributes to diffraction dissociation into high masses, shown in Fig. 4 (a). The corresponding triple-Regge diagram is shown in Fig. 4 (b). Note that the bare Pomeron occurs on the left-hand side of the diagram, because we are considering events with only one large rapidity gap. It is not quite so obvious whether to take bare or physical Pomerons on the right-hand side of the diagram; as we discussed in Sec. II C, it is a question of a perturbative approach vs a self-consistent approach. For logical simplicity we shall regard these as physical Pomerons, but for calculational simplicity shall assume that they can be adequately approximated by effective Pomeron poles. In this approximation one obtains the usual

triple-Regge formula,^{22,23}

$$\frac{d\sigma}{dM^2 dt} = \frac{s_0}{s^2} \frac{G_P^0(t)}{16\pi} \left(\frac{s}{M^2}\right)^{2\alpha_P(t)} \left(\frac{M^2}{s_0}\right)^{\alpha_0(0)}, \quad (3.1)$$

where

$$G_P^0(t) \equiv \beta_{bbP}^2(t) \beta_{aa0}(0) |\xi_P(t)|^2 g_{PP0}(t), \quad (3.2)$$

where $g_{PP0}(t)$ is the function describing the vertex of two Pomerons and one bare Pomeron. For simplicity we shall discuss only the experimentally interesting case $b = b'$, single dissociation into a high-mass state, but Eq. (3.1) is also applicable with only modification of the subscripts to the more general dissociation with one large and one small mass shown in Fig. 4.

In order to calculate the contribution of Eq. (3.1) to the total cross section we need to integrate over the kinematically allowed range of t , and over a range $M_0^2 < M^2 < rs$. The lower limit should be chosen high enough to make Pomeron dominance an adequate approximation in Eq. (3.1). The $M < M_0$ contribution has already been discussed in Sec. II b, and is included in Eq. (2.7). The upper limit comes from the fact that we are considering terms with one large rapidity gap. If we let Δ be the minimum gap length which defines a large rapidity gap, then this implies $M^2 < rs$, where

$$r \approx \exp(-\Delta). \quad (3.3)$$

We therefore wish to perform the integration

$$\int_{M_0^2}^{rs} dM^2 \int_{-\infty}^{t_{\min}} dt \frac{d^2\sigma}{dM^2 dt} \equiv \sigma_{D,M > M_0}, \quad (3.4)$$

where

$$t_{\min} \approx -m_b^2 (M^2/s)^2, \quad (3.5)$$

and where the lower limit of the t integration has been replaced by $-\infty$. It is also apparent that it is consistent with our approximation scheme to replace t_{\min} by zero. We can then carry out the M^2 integration to obtain²⁴

$$\begin{aligned} \sigma_{D,M > M_0}(s) &= \frac{1}{16\pi} \left(\frac{s}{s_0}\right)^{\alpha_0(0)-1} \\ &\times \int_{-\infty}^0 dt \frac{G_P^0(t)}{\epsilon(t)} \left[r^{\epsilon(t)} - \left(\frac{s}{M_0^2}\right)^{-\epsilon(t)} \right], \end{aligned} \quad (3.6)$$

where

$$\epsilon(t) \equiv 1 + \alpha_0(0) - 2\alpha_P(t). \quad (3.7)$$

If we now assume a linear trajectory for small t , with $\alpha_0(0) \approx \alpha_P(0) \approx 1$,

$$\alpha_P(t) \approx 1 + \alpha'_P t, \quad (3.8)$$

we obtain

$$\begin{aligned} \sigma_{D,M > M_0}(s) &= \frac{1}{32\pi\alpha'_P} \\ &\times \int_{-\infty}^0 dt \frac{G_P^0(t)}{t} \left[\left(\frac{s}{M_0^2}\right)^{2\alpha'_P t} - r^{-2\alpha'_P t} \right]. \end{aligned} \quad (3.9)$$

For the physically interesting case that the t dependence of $G_0(t)$ is sufficiently steep to permit expansion about $t=0$ of the term in brackets in Eq. (3.9), one obtains the result

$$\sigma_{D,M > M_0}(s) \approx \frac{\bar{G}_P^0}{16\pi} \ln \frac{rs}{M_0^2}, \quad (3.10)$$

where

$$\bar{G}_P^0 \equiv \int_{-\infty}^0 dt G_P^0(t). \quad (3.11)$$

We see from Eq. (3.10) that our perturbation scheme predicts that the cross section for single diffractive dissociation into high masses should, to good approximation, show a logarithmic rise with energy over a finite energy range, regardless of the functional form of $G_P^0(t)$. The detailed functional form will, however, affect the asymptotic behavior for very large s . If, for example, we choose

$$G_P^0(t) = -G'_0 t e^{bt}, \quad (3.12a)$$

then we find that

$$\sigma_{D,M > M_0}(s) = \frac{G'_0 \ln(rs/M_0^2)}{16\pi [b + 2\alpha'_P \ln(s/M_0^2)] [b - 2\alpha'_P \ln r]}. \quad (3.12b)$$

If, on the other hand, we choose

$$G_P^0(t) = G_0 e^{bt}, \quad (3.13a)$$

then we find that

$$\sigma_{D,M > M_0}(s) = \frac{G_0}{32\pi\alpha'_P} \ln \frac{b + 2\alpha'_P \ln(s/M_0^2)}{b - 2\alpha'_P \ln r}. \quad (3.13b)$$

Although the choice in Eq. (3.12) has been a popular one because it leads asymptotically to a constant cross section and thereby avoids difficulty with the Froissart bound, the choice among functional forms of $G_0(t)$ may not be of great importance at energies available today. Both Eq. (3.12b) and Eq. (3.13b) reduce to Eq. (3.10) provided that

$$2\alpha'_P \ln(s/M_0^2) \ll b, \quad (3.14)$$

which seems likely to be satisfied at NAL and perhaps ISR energies, because of the small values reported for the slope of the Pomeron trajectory.

To summarize, we have calculated the cross section for single diffractive dissociation into

high-mass states in the approximation of pole dominance of the Pomanchuk singularity, and found that it rises like $\ln s$ as long as Eq. (3.14) is satisfied. It will be very interesting to see if the reported rise in the total cross section is associated with this term.^{8,9} If so, it should persist only until Eq. (3.14) is violated, or until higher-order terms become important.

B. Multiplicity Distribution in High-Mass Diffractive Dissociation

Factorization of the Pomeron pole, whether bare or effective, was one of the essential ingredients leading to Eq. (3.1). If instead of examining the total diffractive dissociation cross section we study the partial cross section for dissociation into n particles (Fig. 5), we still can use the factorization of the Pomeron pole. This allows us to write the cross section for single dissociation into a definite number of particles n as

$$\frac{d^2\sigma_{ab}^n}{dM^2 dt} = \frac{|\beta_{bP}(t)|^2}{16\pi s^2} \left(\frac{s}{M^2}\right)^{2\alpha_P(t)} M^2 \sigma_{aP}^n(M^2, t), \tag{3.15}$$

where $\sigma_{aP}^n(M^2, t)$ is the cross section for production of n particles from hadron a and a Pomeron (see Fig. 5). We further assume that hadron-Pomeron cross sections are similar to hadron-hadron cross sections. In order to calculate a cross section which is more easily measured, let us now consider events with at least one large rapidity gap, i.e., Fig. 5 rather than Fig. 4. In this case all three Pomerons are physical.

Consider now the average multiplicity of hadrons of type i produced in diffractive dissociation of hadron a into a state of mass M at a momentum transfer t (see Fig. 5):

$$\begin{aligned} \langle n_a^i(M^2, t) \rangle_D &\equiv \sum_{n_i} n_i \frac{d^2\sigma_{ab}^{n_i}}{dM^2 dt} / \frac{d^2\sigma_{ab}}{dM^2 dt} \\ &= \sum_{n_i} n_i \sigma_{ab}^{n_i}(M^2, t) / \sigma_{aP}(M^2, t). \end{aligned} \tag{3.16}$$

Note that $\langle n_a^i \rangle_D$ is defined with respect to the corresponding diffractive cross section, not the total

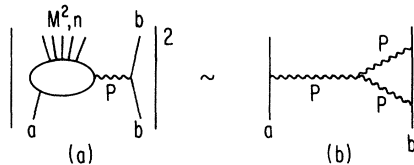


FIG. 5. Process with at least one large rapidity gap, with a large mass on one side of the gap and a small one on the other (single diffractive dissociation into a high-mass state).

cross section. The factorizable-Pomeron hypothesis permits one to apply the standard multiperipheral or Mueller-Regge arguments²⁵ to infer the asymptotic behavior for large M^2 ,

$$\begin{aligned} \sigma_{aP}(M^2, t) \langle n_a^i(M^2, t) \rangle &\sim [\beta_{aP}^{(0)} g_P(t) A^i \ln M^2 + B_a^i(t)] \\ &+ O[(M^2)^{\alpha_M(0)-1}], \end{aligned} \tag{3.17}$$

where $g_P(t)$ is the triple-Pomeron coupling defined in Ref. 7, and to infer that the Pomeron-hadron cross section should behave as

$$\sigma_{aP}(M^2, t) \sim \beta_{aP}(0) g_P(t) + O[(M^2)^{\alpha_M(0)-1}], \tag{3.18}$$

where $\alpha_M(t)$ represents the highest-ranking secondary trajectory. For any desired level of accuracy there exists a value M_0 such that for $M > M_0$ the second term in Eqs. (3.17) and (3.18) representing the contribution of secondary trajectories, can be neglected. We then obtain the simple result: The average multiplicity of hadrons of type i produced in diffraction dissociation into a state of mass M , where $M > M_0$, rises linearly with $\ln M^2$,

$$\langle n_a^i(M^2, s, t) \rangle_D = A^i \ln M^2 + B_a^i(t), \tag{3.19}$$

with the same coefficient A^i (independent of s, t , and incident particle type) found in the average multiplicity measured in hadronic reactions.

The average multiplicity for diffraction dissociation into states in a range of $M_0^2 \leq M^2 \leq rs$ at a given value of t can also be calculated, with the result

$$\begin{aligned} \langle n_a^i(M_0^2 \leq M^2 \leq rs, t) \rangle_D &\sim A^i \frac{\int d(\ln M^2) (M^2)^{\epsilon(t)} \ln M^2}{\int d(\ln M^2) (M^2)^{\epsilon(t)}} \\ &+ \dots \end{aligned} \tag{3.20a}$$

$$\begin{aligned} &\approx \frac{1}{2} A^i \ln \frac{rs}{M_0^2} + C_a^i(t) + \dots \end{aligned} \tag{3.20b}$$

Note the coefficient $\frac{1}{2} A^i$, half the coefficient found in the average multiplicity measured in hadronic reactions. The simplification from Eq. (3.20a) to Eq. (3.20b) has been accomplished by taking the approximation $\epsilon(t) \approx 0$, where $\epsilon(t)$ is defined in analogy to Eq. (3.7) as

$$\epsilon(t) \equiv 1 + \alpha_P(0) - 2\alpha_P(t). \tag{3.21}$$

Provided that this approximation is adequate over the region in which $G_P(t)$ is significantly different from zero, one can integrate over t to obtain finally

$$\langle n_a^i(M_0^2 \leq M^2 \leq rs) \rangle_D \sim \frac{1}{2} A^i \ln \frac{rs}{M_0^2} + \bar{C}_a^i + \dots \tag{3.22}$$

The above result has been derived in the no-

shrinkage approximation of Eq. (3.14). Just as in the discussion preceding Eq. (3.13), it is possible to relax this approximation if a definite functional form is assumed for $G_P(t)$. If, for example, the choice in Eq. (3.13a) is taken, one finds

$$\langle n_a^i(M_0^2 \leq M^2 \leq rs) \rangle_D \sim A^i \left\{ \frac{b}{2\alpha'_P} + \ln \frac{s}{M_0^2} - \ln \frac{rs}{M_0^2} \left[\ln \frac{b + 2\alpha'_P \ln(s/M_0^2)}{b - 2\alpha'_P \ln r} \right]^{-1} \right\}, \quad (3.23)$$

which, in the limit of Eq. (3.14), reduces to Eq. (3.22).

The results above follow directly from the factorizable-Pomeron hypothesis, and therefore provide definitive model-independent tests of that hypothesis. In order to clarify the origin of these results, it is helpful to examine a simple model, which is offered in the spirit of exhibiting the simplest possible multiperipheral-type model of diffractive production. Like the Chew-Pignotti model, of which it is a simple extension, it should have illustrative value, but it must be recognized as an oversimplification rather than as a definitive prediction of the multiperipheral picture.

We construct the model by taking $\sigma_{aP}^n(M^2)$ to be the simplest multiperipheral type of distribution, a Poisson distribution,

$$\sigma_{aP}^n(M^2, t) = \beta_{aP}(0) g_P(t) \frac{[A \ln(M^2/s_a)]^n}{n!} e^{-A \ln(M^2/s_a)}. \quad (3.24)$$

Such a distribution has been found in Ref. 1 to be a good fit to ~80% of the inelastic production in the range 100–300 GeV. The remainder of the production was taken, in that fit, to be diffractive. For simplicity we ignore the diffractive component in Eq. (3.24); this corresponds to calculation of the cross section for events with only one large rapidity gap, but such differences are not large enough to worry about in the context of the present crude model. The scale factor s_a is a parameter of the model, and need not necessarily have the same value as that needed to fit the multiplicity distribution in p - p collisions. This reflects the fact that the parameter B_a^i in Eq. (3.19) depends on the nature of the incident particles.

Substituting Eq. (3.24) in Eq. (3.15) one finds

$$\frac{d\sigma_{ab}^n}{dM^2 dt} = \frac{G_P^{ab}(t)}{16\pi s^2} \left(\frac{s}{M^2} \right)^{2\alpha_P(t)} \left(\frac{M^2}{s_a} \right)^{1-A} \frac{[A \ln(M^2/s_a)]^n}{n!}. \quad (3.25)$$

That is, the multiplicity distribution of hadrons produced diffractively into a state of high mass M is Poisson-distributed in this model. Again, we can integrate over a range of M , $M_0^2 \leq M^2 \leq rs$, to

obtain, for $\epsilon(t) \approx 0$ and for $n > 0$ (assuming $M_0^2 \leq s_a$),

$$\int_{M_0^2}^{rs} \frac{d^2\sigma_{ab}^n}{dM^2 dt} dM^2 \approx \frac{G_P^{ab}(t)}{16\pi A} P(n+1, A \ln \frac{rs}{s_a}), \quad (3.26)$$

where $P(n, x)$ is an incomplete gamma function.^{26,27} Integrating over t , we then obtain the following model for the cross section for the production of n particles by single diffractive dissociation:

$$\sigma_D^n(s) \approx \frac{\bar{G}_P^{ab}}{16\pi A} P(n+1, A \ln \frac{rs}{s_a}) + (a \leftrightarrow b). \quad (3.27)$$

The two terms represent the dissociation of particle a and particle b , respectively. The contribution of low-mass resonances, which are not included in Eq. (3.24), should be added to Eq. (3.27) to form the complete diffractive-dissociation cross section. Although this contribution is not well known, it will affect only the low-multiplicity cross sections. For this reason, and because of the approximations which led to Eq. (3.27), we propose it as a reasonable model only for higher values of n .

The distribution given by Eq. (3.27) is well known to physicists; it is just the χ^2 distribution with the "number of degrees of freedom" $\frac{1}{2}\nu = n+1$, and with $\frac{1}{2}\chi^2 = A \ln(rs/s_a)$. It is shown in Fig. 6 for the case appropriate to $E_L = 1500$ GeV. As is characteristic of χ^2 distribution, it falls to half its maximum at $n \approx A \ln(rs/s_a)$, which is just the average multiplicity of the nondiffractive component,

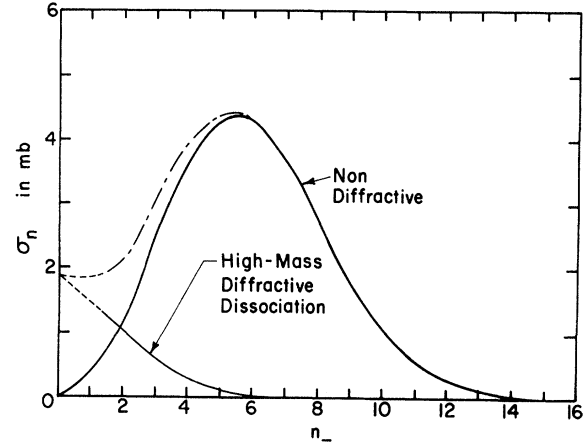


FIG. 6. High-mass ($M > M_0$) diffractive contribution to the multiplicity distribution in p - p scattering at $E_L = 1500$ GeV [$\sqrt{s} = 53$ GeV, according to the model given by Eq. (3.27)]: The nondiffractive contribution is a Poisson distribution from the fits of Ref. 1. The parameters of the diffractive term are taken to be $M_0^2 = s_a = 15$, $A = 1.0$, and $\bar{G}_P/16\pi = 1$ mb. The diffractive contribution is shown as a dashed line for small n , to signify that the model should not be used in this region because of approximations made and because the contribution of diffractive dissociation into low masses must be added in this region.

shifted downward by a constant amount. Its mean is given (for $s_a \geq M_0^2$) by

$$\langle n^i \rangle_{D, M > M_0} \approx \frac{1}{2} [\langle n^i \rangle_{\text{SRC}} - A^i \Delta]. \quad (3.28)$$

This is consistent with Eq. (3.22), but in addition makes a specific estimate of the constant term. It makes the appropriate kinematical correction (reduced length of rapidity interval), but ignores the possible dynamical effects which could lead to different constant terms.

No data on high-mass diffractive dissociation are yet available for comparison with the predictions above. The model-dependent separation of the diffractive component in Ref. 1 gave detailed information (not all of which was published) which is shown in Table I. Note that the multiplicity distribution of the diffractive component is broadening with increasing energy, but these data are too model-dependent and fragmentary to be taken as confirmation.

IV. HIGHER-ORDER TERMS: SMALL PARAMETERS

A. Double Diffractive Dissociation into High-Mass States

Consider those events characterized by one large rapidity gap, leading to large missing masses on both sides of the gap, $s_1 > M_0^2$ and $s_2 > M_0^2$, shown in Fig. 7. In the multi-Regge limit of large gap size and large s_1 and s_2 , this process contributes⁷

$$\frac{d\sigma}{dt ds_1 ds_2} \sim \frac{g_{PP_0}^2(t) \beta_{aa_0}(0) \beta_{bb_0}(0)}{16\pi s^2} \left(\frac{ss_0}{s_1 s_2} \right)^{2\alpha_P(t)} \times (s_1 s_2)^{\alpha_0(0)}. \quad (4.1)$$

As in Sec. III, $\alpha_0(0)$ occurs as the exponent of s_1 and s_2 because we are limiting our attention to events with only one large rapidity gap. Hence, the two blobs in Fig. 7 are governed by the same singularities as the SRC part of the cross section.

Performing the integrals over s_1 , s_2 , and t with the same approximation $\epsilon(t) \approx 0$ as in Sec. III, one finds for the contribution to the total cross section

$$\sigma_{DD, M > M_0} \approx \bar{\eta}_P \beta_{aa_0}(0) \beta_{bb_0}(0) \frac{1}{2} \left(\ln \frac{rs_0}{M_0^4} \right)^2, \quad (4.2)$$

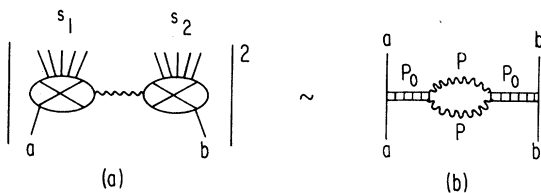


FIG. 7. Process with one large gap, producing two large-mass clusters (double diffractive dissociation into high masses).

where

$$\bar{\eta}_P \equiv \frac{1}{16\pi} \int_{-\infty}^0 dt g_{PP_0}^2(t). \quad (4.3)$$

The parameter $\bar{\eta}_P$ is very similar to the parameter $\eta_P \equiv g_{PP_0}^2(0)/[32\pi\alpha'_P(0)]$ introduced by Abarbanel *et al.*,⁷ but is more appropriate to the energy range and approximation scheme we are considering; that is, we are concentrating on an energy range (appropriate to today's accelerators) in which one can approximately neglect shrinkage [Eq. (3.14)], whereas Abarbanel *et al.* tacitly assumed the energy to be high enough that the slope of the Pomeron trajectory controlled the t dependence.

The small dimensionless parameter $\bar{\eta}_P$ arises in higher-order terms whenever a Pomeron bubble, as in Fig. 7(b), is linked to a bare Pomeron on both ends. Other types of diagrams in which two Pomerons connect to an external line involve $(\bar{\eta}_P)^{1/2}$. It is convenient, then, to define as our basic expansion parameter

$$\lambda_P \equiv (\bar{\eta}_P)^{1/2}. \quad (4.4)$$

We could now proceed to calculate other higher-order contributions to the total cross section and catalog them according to their order in λ_P . The task is complicated, however, by our ignorance of the t dependences involved. We cannot compare, for example, elastic scattering, single diffractive dissociation, and double diffractive dissociation without knowledge of the t dependence of $\beta(t)$ and $g_{PP_0}(t)$.

Since differences in t dependence seem unlikely to lead to order-of-magnitude differences among cross sections, it is useful to catalog the various terms under the assumption that all of them have roughly the same t dependence, which we characterize by slope parameters b_i . In this approximation one finds

$$\sigma_T \approx \beta^2, \quad (4.5a)$$

$$\sigma_{el} \approx \frac{\beta^4}{16\pi b_1}, \quad (4.5b)$$

$$\sigma_{D, M > M_0} \approx \frac{\beta^3 g_{PP_0}}{16\pi b_2} \left(\ln \frac{rs_0}{M_0^2} \right), \quad (4.5c)$$

$$\sigma_{DD, M > M_0} \approx \frac{\beta^2 g_{PP_0}^2}{16\pi b_3} \frac{1}{2} \left(\ln \frac{rs_0}{M_0^4} \right)^2. \quad (4.5d)$$

If, for the purpose of order-of-magnitude estimate, we take all the b_i 's to be roughly equal, then

$$\lambda_P^2 \approx \frac{g_{PP_0}^2}{16\pi b}, \quad (4.6)$$

and one finds the probabilities


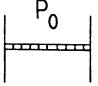

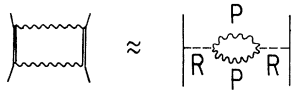
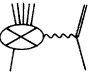
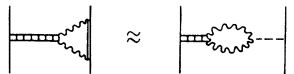
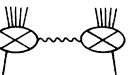
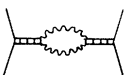
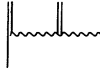
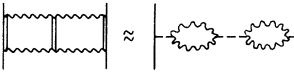
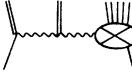
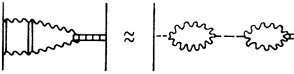

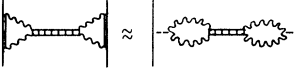
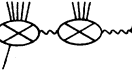
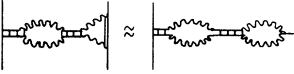
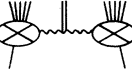
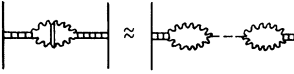
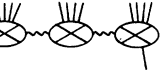
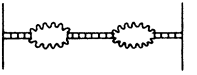
Process σ_i	Mueller-Regge Diagram	Order of σ_i/σ_T
1) 		λ_0^2
2) 		λ_D^2
3) 		$\lambda_0 \lambda_D \lambda_P (\gamma - \Delta - \Delta_f) \theta ()$
4) 		$\frac{1}{2} \lambda_0^2 \lambda_P^2 (\gamma - \Delta - 2\Delta_f)^2 \theta ()$
5) 		$\lambda_D^2 \lambda_I^2 (\gamma - 2\Delta) \theta ()$
6) 		$\frac{1}{2} \lambda_0 \lambda_D \lambda_I^2 \lambda_P (\gamma - 2\Delta - \Delta_f)^2 \theta ()$
7) 		$\lambda_D^2 \frac{1}{2} \lambda_P^2 (\gamma - 2\Delta - \Delta_f)^2 \theta ()$
8) 		$\lambda_0 \lambda_D \frac{1}{3!} \lambda_P^3 (\gamma - 2\Delta - 2\Delta_f)^3 \theta ()$
9) 		$\frac{1}{3!} \lambda_0^2 \lambda_I^2 \lambda_P^2 (\gamma - 2\Delta - 2\Delta_f)^3 \theta ()$
10) 		$\frac{1}{4!} \lambda_0^2 \lambda_P^4 (\gamma - 2\Delta - 3\Delta_f)^4 \theta ()$

FIG. 8. Relative order of all contributions to the total cross section with zero, one, or two large rapidity gaps. The parameters are defined, and estimates of their values are given, in Sec. IV.

$$\frac{\sigma_{el}}{\sigma_T} \approx \frac{\beta^2}{16\pi b} \equiv \lambda_{el}^2, \quad (4.7a)$$

$$\frac{\sigma_{D, M > M_0}}{\sigma_T} \approx \lambda_P \lambda_{el} \ln \frac{\gamma S}{M_0^2}, \quad (4.7b)$$

$$\frac{\sigma_{DD, M > M_0}}{\sigma_T} \approx \frac{1}{2} \left(\lambda_P \ln \frac{\gamma S S_0}{M_0^4} \right)^2. \quad (4.7c)$$

And, letting the symbol $\sigma_{DD, M < M_0}$ stand for all diffractive dissociation into clusters of mass $M < M_0$, including elastic scattering, we define

$$\sigma_{DD, M < M_0}^{2b} / \sigma_T \equiv (\lambda_D^{ab})^2. \quad (4.7d)$$

Continuing in a similar manner, we are able to fill in the catalog in Fig. 8, except for the necessity of defining a third parameter, to which we now turn.

B. Multiple Diffraction Dissociation into Low-Mass States

The process shown in Fig. 9 has two large rapidity gaps, but does not involve our parameter λ_P because there is no production of high-mass states. It is, however, believed to be small, since experimental searches have failed to find evidence for such a process.²⁸ These searches have, however, not yet been carried out at very high energies. It seems unlikely that the smallness of this process is unrelated to the small parameter λ_P ; nevertheless, we know of no way to make the connection with our present level of S-matrix technology and are forced to introduce another parameter to characterize the strength of the internal vertex in Fig. 9.

Alternatively, one can use duality ideas to relate resonance production in low-mass diffractive dissociation to the exchange of non-Pomeron Regge trajectories. Consider, for example, low-mass diffractive dissociation (including elastic scattering), shown in Fig. 3. If we assume that the sum over low-mass resonances can be approximated by exchange of a Regge pole, then low-mass dissociation can be represented by the diagram in Fig. 10. The Regge pole R is a "bare" pole with vacuum quantum numbers (perhaps a bare P'). Note the similarity between Figs. 10 and Fig. 7; high-mass dissociation involves Pomeron exchange where low-mass dissociation involves R exchange.

If one evaluates low-mass dissociation from Fig. 10(b) in the same approximation as we evaluated high-mass dissociation in Eq. (4.2), one finds

$$\sigma_{DD, M < M_0} = \bar{\eta}_R \beta_{aaR}(0) \beta_{bbR}(0) L^2, \quad (4.8a)$$

where L is the inclusive correlation length

$$L = [1 - \alpha_R(0)]^{-1} \quad (4.8b)$$

and where

$$\lambda_R^2 \equiv \bar{\eta}_R \equiv \frac{1}{16\pi} \int_{-\infty}^0 dt g_{PPR}^2(t). \quad (4.8c)$$

Note that $\bar{\eta}_R$ is defined analogously to the triple-Pomeron coupling parameter $\bar{\eta}_P$, which we defined in Eq. (4.3). Similarly, one can define a parameter $\eta_R \equiv g_{PPR}^2(0)/[32\pi\alpha'_P(0)]$ analogous to η_P of Abarbanel *et al.*,⁷ but $\bar{\eta}_R$ should be more useful at NAL-

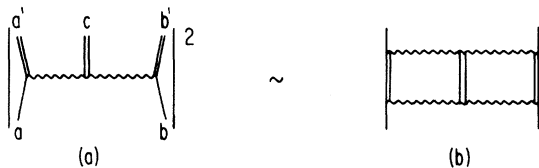


FIG. 9. Process with two large rapidity gaps, leading to low-mass clusters only.

ISR energies for the reasons stated above in connection with $\bar{\eta}_P$.

In comparing low-mass and high-mass dissociation, Eq. (4.8) vs Eq. (4.2), one sees that the factor $\ln^2 s$ has been replaced by L^2 . This can easily be understood as a consequence of the amount of phase space available in the rapidity variable y . Low-mass dissociation products are confined on the average to a region whose length is less than one correlation length L , while high-mass dissociation products spread over the entire available phase space Y (minus threshold factors which we discuss next).

In forming Fig. 8 we have used the abbreviation

$$\lambda_f^2 \approx \lambda_R^2 L. \quad (4.9)$$

Moreover, one sees by comparing Eq. (4.7d) and (4.8) that

$$(\lambda_D^{ab})^2 = \frac{\beta_{aaR}(0)\beta_{bbR}(0)}{\beta_{aaP}(0)\beta_{bbP}(0)} \lambda_R^2 L^2. \quad (4.10)$$

Finally, we define

$$\lambda_a^0 = \frac{\beta_{aa0}(0)}{\beta_{aaP}(0)}, \quad (4.11a)$$

so that

$$\frac{\sigma_{ab}^{SRG}}{\sigma_{ab}^{tot}} \sim \lambda_a^0 \lambda_b^0 \quad (4.11b)$$

C. Threshold Factors

Looking back at our estimate of double dissociation into high masses, Eq. (4.2), it is instructive to rewrite the logarithm as follows: Recall that the parameter r is related to the minimum rapidity gap,

$$r \approx e^{-\Delta}. \quad (4.12)$$

Then we further define Δ_f , the minimum rapidity spread which defines a high-mass cluster

$$\frac{M_0^2}{s_0} = e^{\Delta_f}. \quad (4.13)$$

Finally, choose s_0 such that the available phase space in rapidity, Y , is given by

$$\frac{s}{s_0} = e^Y. \quad (4.14)$$

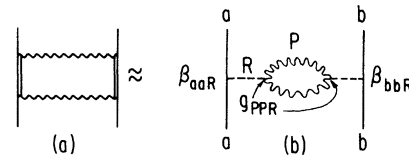


FIG. 10. Representation of low-mass diffractive dissociation, using duality assumption to replace sum over resonances by Reggeon exchange.

The usual choice is $s_0 = m_a m_b$, but when working at fixed transverse momentum with final-state particles of mass m it is appropriate to take $s_0 = \mu^2 = m^2 + p_\perp^2$. With the above definitions one can rewrite Eq. (4.2) in the form

$$\sigma_{DD, M > M_0} \approx \bar{\eta}_P \beta_{aa0}(0) \beta_{bb0}(0)^{\frac{1}{2}} (Y - 2\Delta_f - \Delta)^2 \times \theta(Y - 2\Delta_f - \Delta), \quad (4.15)$$

where we have explicitly written the θ function implicit previously. The meaning of the θ function is evident: Double dissociation with a minimum rapidity gap Δ into two high-mass clusters of minimum spread Δ_f cannot occur until the available rapidity is $Y \geq 2\Delta_f + \Delta$.

It is especially easy to see how to generalize Eq. (4.15) to more complicated processes if one uses DeTar's simplified phase space in terms of rapidities.¹⁴ Consider a distribution of rapidities, such as shown in Fig. 2, divided into an arbitrary number of large-mass clusters, small-mass clusters, and large rapidity gaps. Suppose that rapidities of particles within clusters have been integrated over, and the sums have been carried out over the number of particles n_1, n_2 , etc., within clusters. Assume further, as we have been assuming throughout this paper, that these sums and integrals within clusters build up bare Pomerons, which we take to have intercepts approximately equal to unity. In this case the cross section resulting from a configuration such as Fig. 2 is given by

$$\sigma \propto \int_{\Delta_1} dx_1 \cdots \int_{\Delta_{n+1}} dx_{n+1} \delta(Y - \sum x_i), \quad (4.16)$$

where either $\Delta_i = \Delta$ or $\Delta_i = \Delta_f$, as appropriate to the given configuration. Changing variables to $z_i = x_i - \Delta_i$ one finds

$$\sigma \propto \int_0 dz_1 \cdots \int dz_{n+1} \delta(Y - \sum \Delta_i - \sum z_i) \propto \frac{1}{n!} (Y - n_f \Delta_f - n_g \Delta)^n \theta(Y - n_f \Delta_f - n_g \Delta), \quad (4.17)$$

where

$$n = n_f + n_g - 1,$$

and where n_f = number of large-mass clusters and n_g = number of large rapidity gaps.

The threshold factors found above can lead to important physical phenomena, such as oscillatory behavior of cross sections. It is not obvious from our derivation, however, that they correspond to any real physics, since they have entered via definitions. If we choose to focus our attention on the probability for observing events with n rapidity gaps of minimum size Δ , then clearly such events will not occur until $Y > n\Delta$. Nevertheless, Chew

and Snider,²⁹ and Goldberger, Silverman, and Tan,³⁰ and Misheloff,³¹ have observed that such threshold effects do indeed occur in multiperipheral models, and Chew⁹ has argued that threshold effects and complex poles are essential to the understanding of rising total cross sections in perturbative approaches such as we are expounding.

This discussion of threshold factors completes the list of ingredients needed to make order-of-magnitude estimates of high-order terms in our perturbation expansion. These estimates are listed in Fig. 8.

D. Estimates of Parameters

The magnitudes of the parameters we have introduced are not well known experimentally. In this section we shall attempt rough estimates, based on NAL and ISR data on proton-proton scattering.

The best known of the parameters is λ_{el} . The ratio of elastic to total cross section is not varying appreciably over the NAL-ISR range; the measured value is in the range

$$\lambda_{el}^2 \equiv \sigma_{el}/\sigma_T = 0.17-0.18. \quad (4.18)$$

The ratio of SRC to total cross section is found in two-component fits to be $\approx 0.6-0.7$, implying $\lambda_0 \approx 0.8$. In making the rough estimates of this section, we shall set $\lambda_0 \approx 1$.

The parameter λ_D^2 , which is the ratio of elastic plus low-mass dissociation cross sections to the total cross section, is not well known. Adding in a reasonable guess for low-mass dissociation, we shall take $\lambda_D^2 \approx \frac{1}{4}$. Even less is known about the parameter $\bar{\eta}_P = \lambda_P^2$, but data are beginning to accumulate on diffraction dissociation into high masses which will eventually determine this parameter. If, however, one makes the hypothesis that the rising proton-proton total cross section reported at the ISR¹² is a result of high-mass diffractive dissociation,^{8,9} one finds that the observed rise implies (see Fig. 8)

$$\lambda_P \lambda_P = \frac{1}{\sigma_T} \frac{d\sigma_{D, M > M_0}}{d \ln s} \approx \frac{1}{40}. \quad (4.19)$$

This gives the estimate $\bar{\eta}_P \approx 0.0025$, or $\lambda_P \approx \frac{1}{20}$. Finally, the parameter λ_R^2 , which measures the strength of multiple low-mass dissociation, is related by Eq. (4.11) to λ_D , L , and Regge residues. If we identify R with P' , and take P and P' residues to be roughly equal, we have $\lambda_R^2 \approx \frac{1}{16}$, and hence $\lambda_{P'}^2 \approx \frac{1}{8}$.

Although $\lambda_R^2 \gg \lambda_P^2$, these estimates of both parameters are small enough to make the perturbation expansion seem reasonable. It should be

noted from Fig. 8 (or from the model discussed in Sec. V) that the higher-order terms are formed by adding internal clusters to diagrams 1, 2, and 3; they therefore form an expansion in powers of λ_R^2 and λ_P^2 , not in powers of λ_P or λ_D .

It is interesting to compare these estimates with triple-Regge analyses of high-mass dissociation. The parameters λ_P and λ_R measure the strength of triple-Pomeron and PPR vertices, respectively. Using the same rough approximation of setting ratios of slope parameters and external Regge vertices equal to unity, one expects the rough proportionality

$$\frac{G_{PPP}(t)}{G_{PPR}(t)} \approx \frac{\lambda_P}{\lambda_R}. \quad (4.20)$$

Our estimate above gives $\lambda_P/\lambda_R \approx \frac{1}{5}$, whereas Sannes *et al.*²³ find $G_{PPP}/G_{PPR} = 0.24$ at $t = -0.33$ and 0.25 at $t = -0.45$.

Using the above estimates, one finds that only diagrams 1, 2, 3, and 5 of Fig. 8 contribute significantly at ISR energies. Diagram 5 is about equal to diagram 3 [which implies an overestimate in Eq. (4.19)]; that is, of the order of 1 mb. It would be very interesting to search for this process at the ISR.

V. SIMPLIFIED MULTI-REGGE MODEL

A. The Model

To clarify the ideas presented in this paper, we shall now discuss them in the context of a highly simplified multi-Regge model of the $t=0$ J -plane amplitude.^{4,11,32,33} The model is characterized by the following assumptions:

(1) Only two types of input Regge exchanges are considered, Pomeron and meson. The latter is, as usual, regarded as representing the average effect of all secondary trajectories.

(2) The external couplings G are considered to be independent of the internal couplings, g , shown in Fig. 11. For simplicity, adjacent Pomeron exchange is excluded.

(3) Degenerate kernels are assumed in order to reduce integral equations to algebraic equations

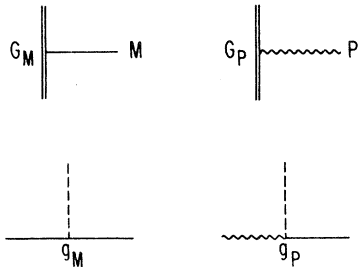


FIG. 11. Coupling constants in model of Sec. V.

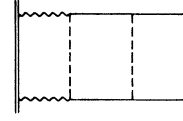


FIG. 12. Typical absorptive amplitude in model, corresponding to Eq. (5.1).

in the standard manner, and AFS cuts are replaced by effective poles. The two-Pomeron cut is replaced by a pole at $J = \beta_P$, where $\beta_P \leq 2\alpha_P - 1$, and the two-meson cut is replaced by a pole at $J = \beta_M$, where $\beta_M \leq 2\alpha_M - 1$. The meson-Pomeron interference term is neglected.

As an example of the construction of a multi-Regge amplitude from these rules, the process in Fig. 12 yields the following J -plane amplitude at $t=0$:

$$A(J) = G_P^2 \frac{1}{J - \beta_P} g_P^2 \frac{1}{J - \beta_M} g_M^2 \frac{1}{J - \beta_M} G_M^2. \quad (5.1)$$

B. Calculation of $A(J)$

We proceed now to calculate the complete J -plane absorptive amplitude $A(J)$ by summing the various contributions. The solution can be found in the literature,³³ but we reproduce the calculation both for completeness and in order to identify the origin of the various contributions. First, the meson-exchange terms shown in Fig. 13 give rise to the following sum:

$$\frac{1}{J - \beta_M} + \frac{g_M^2}{(J - \beta_M)^2} + \frac{g_M^4}{(J - \beta_M)^3} + \dots = \frac{1}{J - \beta_M - g_M^2}. \quad (5.2)$$

The sum of all the diagrams without Pomeron exchange gives rise to the SRC component of the total cross section (in the J plane),

$$A_{\text{SRC}}(J) = \frac{G_M^4}{J - \alpha_0}, \quad (5.3)$$

where

$$\alpha_0 \equiv \beta_M + g_M^2 \quad (5.4)$$

is the position of the J -plane pole in this approximation. We shall call this pole the "bare" Pomeron, and denote it graphically by the small ladder in Fig. 13.

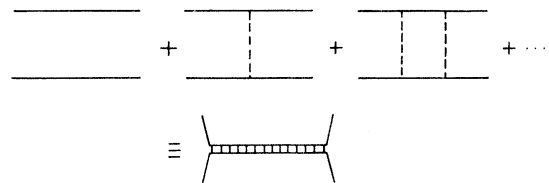


FIG. 13. Diagrams without Pomeron exchange, adding up to bare Pomeron.

The fact that $A_{\text{SRC}}(J)$ has only a single J -plane pole is, of course, a result of the oversimplification of the model. If one wished to make the model realistic enough for use in phenomenology, it would be necessary to add a secondary pole to Eq. (5.3).³⁴ The meaning of a secondary pole as a dual representation of low-mass diffraction dissociation was discussed in Sec. IV B.

Since the remainder of the contributions must have at least one Pomeron link, it is convenient to think of these contributions as a product of three factors: two generalized vertices which themselves contain no Pomeron links, plus a "dressed" Pomeron propagator. The vertex diagrams, shown in Fig. 14, give the following formula:

$$G_P^2 + \frac{G_M^2 g_P^2}{J - \beta_M} + \frac{G_M^2 g_M^2 g_P^2}{(J - \beta_M)^2} + \dots = G_P^2 + \frac{G_M^2 g_P^2}{J - \alpha_0}. \quad (5.5)$$

Finally, we form the "dressed" Pomeron propagator by summing all diagrams which can occur between Pomeron links, as shown in Fig. 15, with the result

$$\frac{1}{J - \beta_P} + \frac{g_P^4}{(J - \beta_P)^2 (J - \alpha_0)} + \dots = \frac{J - \alpha_0}{(J - \alpha_0)(J - \beta_P) - g_P^4}. \quad (5.6)$$

We are now ready to put all this together into an expression for the complete J -plane absorptive amplitude:

$$A(J) = \frac{G_M^4}{J - \alpha_0} + \frac{[G_P^2 + (G_M^2 g_P^2)/(J - \alpha_0)](J - \alpha_0)}{(J - \beta_P)(J - \alpha_0) - g_P^4}, \quad (5.7a)$$

$$= \frac{G_M^4 (J - \beta_P) + 2G_P^2 G_M^2 g_P^2 + G_P^4 (J - \alpha_0)}{(J - \beta_P)(J - \alpha_0) - g_P^4}. \quad (5.7b)$$

We shall now discuss the implications of this expression.

C. Bare and Dressed Pomeron Poles

Note that the bare Pomeron singularity, which appears in $A_{\text{SRC}}(J)$ in Eq. (5.3), is not a singularity of the full absorptive amplitude in Eq. (5.7b). The true singularities occur at $J = \alpha_{\pm}$, where α_{\pm} both satisfy the equation

$$(\alpha_{\pm} - \beta_P)(\alpha_{\pm} - \alpha_0) = g_P^4, \quad (5.8)$$

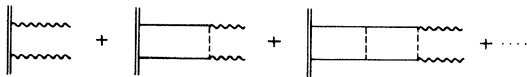


FIG. 14. End of diagram, to left of all Pomeron links.

namely,

$$2\alpha_{\pm} = \alpha_0 + \beta_P \pm [(\alpha_0 - \beta_P)^2 + 4g_P^4]^{1/2}. \quad (5.9)$$

Calculating the residues of these poles, and simplifying them by means of Eq. (5.8), we can write the absorptive amplitude as

$$A(J) = \frac{f_+^2}{J - \alpha_+} + \frac{f_-^2}{J - \alpha_-}, \quad (5.10)$$

where

$$f_+ = \frac{1}{(\alpha_+ - \alpha_-)^{1/2}} [G_M^2 (\alpha_+ - \beta_P)^{1/2} + G_P^2 (\alpha_+ - \alpha_0)^{1/2}], \quad (5.11)$$

$$f_- = \frac{1}{(\alpha_+ - \alpha_-)^{1/2}} [G_M^2 (\beta_P - \alpha_-)^{1/2} - G_P^2 (\alpha_0 - \alpha_-)^{1/2}].$$

The total cross section as a function of s is then

$$\sigma(s) = f_+^2 s^{\alpha_+ - 1} + f_-^2 s^{\alpha_- - 1}. \quad (5.12)$$

What is the interpretation of the two poles α_+ and α_- ? We shall, of course, interpret α_+ as the dressed Pomeron, but the identification of α_- is less obvious. Chew and Snider speculated that it could be identified with the P' trajectory.¹¹ A more conservative approach is to identify it as an effective P - P cut contribution, recognizing that we have been working in an approximation in which cuts are replaced by poles. It is interesting to note, however, that for reasonable values of the parameters in Eq. (5.11) one finds that $f_- \ll f_+$. This is reassuring, because a large value of f_- would contradict the observation that total cross sections are approximately constant through the Serpukhov-NAL energy range.

D. Perturbation Expansion in Powers of g_P^2

Expanding Eq. (5.7) in powers of g_P^2 through terms of order g_P^4 , one finds

$$A(J) = \frac{G_M^4}{J - \alpha_0} + \frac{G_P^4}{J - \beta_P} + \frac{2G_M^2 g_P^2 G_P^2}{(J - \beta_P)(J - \alpha_0)} + \frac{G_M^4 g_P^4}{(J - \beta_P)(J - \alpha_0)^2} + \frac{G_P^4 g_P^4}{(J - \alpha_0)(J - \beta_P)^2} + \dots \quad (5.13)$$

These terms correspond, in the same order as written, to diagrams 1, 2, 3, 4, and 7 in Fig. 8.

The first three terms of Eq. (5.13) can be taken

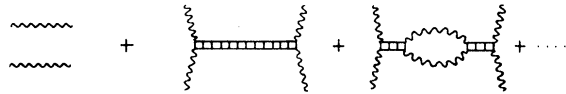


FIG. 15. Sum of all diagrams between Pomeron links.

as a theoretical model for the popular two-component fits to multiplicity distributions.¹⁻³ Transforming them to the s plane one finds

$$\sigma(s) = G_M^4 s^{\alpha_0-1} + G_P^4 s^{\beta_P-1} + 2G_M^2 G_P^2 g_P^2 \frac{s^{\alpha_0-1} - s^{\beta_P-1}}{\alpha_0 - \beta_P} + \dots \quad (5.14)$$

Now, we know from phenomenological fits that α_0 and β_P are not very different in magnitude; there-

fore, a rough approximation consists of taking $\alpha_0 = \beta_P \equiv \beta$. In this case Eq. (5.14) simplifies to

$$\sigma(s) \approx s^{\beta-1} [G_M^4 + G_P^4 + 2G_M^2 G_P^2 g_P^2 \ln s] + \dots \quad (5.15)$$

This approximation can, of course, be valid only over a finite range of energies; it breaks down unless $|\alpha_0 - \beta_P| \ln s \ll 1$. In this approximation it is possible to write down the entire series quite simply:

$$\begin{aligned} \sigma(s) s^{1-\beta} &= (G_M^4 + G_P^4) \left[1 + \frac{1}{2} (g_P^2 \ln s)^2 + \frac{1}{4!} (g_P^2 \ln s)^4 + \dots \right] + 2G_M^2 G_P^2 \left[g_P^2 \ln s + \frac{1}{3!} (g_P^2 \ln s)^3 + \dots \right] \\ &= (G_M^4 + G_P^4) \cosh(g_P^2 \ln s) + 2G_M^2 G_P^2 \sinh(g_P^2 \ln s). \end{aligned} \quad (5.16)$$

Comparing Eq. (5.16) and Fig. 8, one can read off the following correspondence between the parameters:

$$\lambda_P = g_P^2, \quad \lambda_{cl} = \frac{G_P^2}{G_M^2}. \quad (5.17)$$

Since adjacent Pomeron links have been left out of our simplified model and secondary trajectories have been left out of A_{SRC} , we have effectively set $\lambda_f = 0$. There are no threshold factors in Eq. (5.16); again, our simplified model has left them out. In analogy to the work of Chew and Snider,²⁹ we find that they can be reinstated by the simple replacements

$$\frac{1}{J - \beta_P} \rightarrow \frac{e^{-(J - \beta_P)\Delta}}{J - \beta_P}; \quad \frac{1}{J - \beta_M} \rightarrow \frac{e^{-(J - \beta_M)\Delta_f}}{J - \beta_M}. \quad (5.18)$$

The resulting model has complex Regge poles and an oscillating total cross section, as discussed recently by Chew.⁹

ACKNOWLEDGMENTS

In striving for a logically complete presentation of the perturbative basis of two-component models, we have necessarily devoted a large part of this paper to reproducing or reexpressing ideas already in the literature. The basic idea of the existence of a small parameter characterizing inelastic diffractive processes was first recognized by Chew and Pignotti,⁴ and elaborated by Chew and various collaborators.⁵⁻⁷ The new development which led to our work was the success of two-component models of multiplicity distributions at high energies—their relatively small diffractive component calls to mind, and suggests new tests of, the small-parameter idea.

While preparing this manuscript we learned that very similar work is being pursued by Chew,

Bishari, and Koplik. We gratefully acknowledge conversations with them which were very stimulating and very helpful in clarifying the ideas presented in this paper.

APPENDIX

The relationship between σ_{SRC} , defined (theoretically) as containing no Pomeron exchange, and $\sigma^{0,\Delta}$, defined (operationally) as being all events with no rapidity gap greater than Δ , may be examined most easily in terms of some particular model. We will use the same model as used in Sec. V. We will show that for Δ in the correct range the two cross sections have nearly the same energy dependence.

The kernels $K_i(J) = g_i^2 (J - \beta_i)^{-1}$ used in constructing the model in Sec. V resulted from Mellin transforms of s -plane Regge asymptotic amplitudes as follows:

$$K(J) = \int_{s_0}^{\infty} \frac{ds}{s} K(s) \left(\frac{s}{s_0}\right)^{-J},$$

where $K_M(s) = g_M^2 (s/s_0)^{\beta_M}$ for meson exchange and a similar equation holds for Pomeron exchange. These lead to $K_M(J) = g_M^2 / (J - \beta_M)$ and $K_P = g_P^2 / (J - \beta_P)$. Now if we consider generating $\sigma^{0,\Delta}$, a cross section that allows any exchanges but excludes all events with a rapidity gap greater than Δ , we start with a cutoff on the maximum value of the subenergy s at $s = r s_0 = s_0 e^{-\Delta} [s_0$ is defined after Eq. (4.14)]:

$$\begin{aligned} K_{\Delta}(J) &= \int_{s_0}^{r s_0} \frac{ds}{s} g^2 \left(\frac{s}{s_0}\right)^{\beta-J} \\ &= g^2 \frac{1 - e^{-(J-\beta)\Delta}}{J - \beta}. \end{aligned}$$

Although the two exchanges, meson and Pomeron, require a two-channel "integral equation," for our purposes we can most easily study the effect by

considering a one-channel equation where the kernel contains both exchanges, i.e.,

$$K(J) = g_M^2 \frac{1 - e^{-(J-\beta_M)\Delta}}{J-\beta_M} + g_P^2 \frac{1 - e^{-(J-\beta_P)\Delta}}{J-\beta_P}.$$

(The only change we are making by switching to a one-channel equation is to allow adjacent Pomeron exchanges.) Notice that, because of our limit on the subenergy, $K_\Delta(J)$ contains no J -plane singularities. The fact that $g_M^2 \gg g_P^2$ and that $\beta_M \approx 0$ while $\beta_P \approx 1$ means that we must handle the two terms very differently.

After summing diagrams as in Sec. V, one finds that the amplitude $A(J)$ is proportional to $[1 - K(J)]^{-1}$. Thus we are interested in looking for zeros of $K(J) - 1$ near $J=1$, which means for $J \approx \beta_P$. Thus we write

$$K(J) - 1 \approx g_M^2 \frac{1 - e^{-(J-\beta_M)\Delta}}{J-\beta_M} + g_P^2 \Delta - 1,$$

where we have assumed $(J-\beta_P)\Delta \ll 1$ for the region in J which interests us. Now if in addition $g_P^2 \Delta \ll 1$, then

$$K(J) \approx g_M^2 \frac{1 - e^{-(J-\beta_M)\Delta}}{J-\beta_M} - 1$$

and the Pomeron will have little effect on the position of the pole. Now if $(J-\beta_M)\Delta \gg 1$, then the pole will be at the standard place $J = \beta_M + g_M^2$. Thus this requirement can be written $g_M^2 \Delta \gg 1$. If this condition is only weakly satisfied, say, $g_M^2 \Delta \approx 2$, then one can see that the position is approximately given by $J = \beta_M + g_M^2(1 - e^{-g_M^2 \Delta})$ so that the position of the pole only approaches $\alpha_0 = \beta_M^2 + g_M^2$ as $\Delta \rightarrow \infty$. Moreover, the conditions

$$|\alpha_0 - \beta_P| \Delta \ll 1$$

and

$$g_P^2 \Delta \ll 1$$

must be satisfied for the Pomeron not to affect the behavior of $\sigma^{0,\Delta}$. Thus the proper choice for Δ is in the range

$$\frac{1}{g_M^2} \ll \Delta \ll \frac{1}{g_P^2}.$$

The lower limit is just the average spacing in rapidity, $\langle \Delta \rangle = Y/\langle n \rangle$. The upper limit $1/g_P^2$ is quite large; a practical limit is imposed by the desire to keep Δ small enough that events with rapidity gaps greater than Δ have appreciable probability.

It is also possible to gain qualitative understanding of the effect of our rapidity-gap decomposition of the cross section by calculating the probability of large rapidity gaps. In a simplified multi-Regge model, such as the one considered in Sec. V, it is easy to show that the probability of a rapidity gap Δ occurring as a result of the exchange of a trajectory of type i is given by

$$\frac{dP_i(\Delta)}{d\Delta} = g_i^2 e^{-a_i \Delta},$$

where

$$a_i = 1 + \alpha_P(0) - 2\alpha_i(0)$$

[this agrees, to within logarithmic factors associated with neglect of shrinkage, with Eq. (8) of Abarbanel *et al.*⁷]. Thus Pomeron exchange gives rise to a flat distribution in rapidity gap size, whereas secondary trajectories give a distribution falling exponentially with increasing gap size. Hence the cross section $\sigma^{1,\Delta}$, which contains one large rapidity gap, is relatively enriched in probability of Pomeron exchange and therefore is expected to show stronger long-range correlations.

*Work supported in part by the United States Atomic Energy Commission.

†Fellow of the John Simon Guggenheim Foundation.

¹W. Frazer, R. Peccei, S. Pinsky, and C.-I. Tan, Phys. Rev. D **7**, 2647 (1973).

²K. Fialkowski and H. Miettinen, Phys. Lett. **43B**, 61 (1973).

³H. Harari and E. Rabinovici, Phys. Lett. **43B**, 49 (1973).

⁴G. F. Chew and A. Pignotti, Phys. Rev. **176**, 2112 (1968).

⁵G. F. Chew and W. R. Frazer, Phys. Rev. **181**, 1914 (1969).

⁶G. F. Chew, T. W. Rogers, and D. R. Snider, Phys. Rev. D **2**, 765 (1970).

⁷H. D. I. Abarbanel, G. F. Chew, M. L. Goldberger, and L. M. Saunders, Phys. Rev. Lett. **26**, 937 (1971); Ann. Phys. (N.Y.) **73**, 156 (1972).

⁸W. R. Frazer and D. R. Snider, NAL Report No. NAL-Pub-73/15/THY, 1973 (unpublished); Phys. Lett. **45B**, 136 (1973).

⁹G. F. Chew, Phys. Rev. D **7**, 3525 (1973); Phys. Lett. **44B**, 169 (1973).

¹⁰G. F. Chew, Phys. Rev. D **7**, 934 (1973).

¹¹G. F. Chew and D. R. Snider, Phys. Rev. D **1**, 3453 (1970); D **3**, 420 (1971).

¹²J. C. Sens, in proceedings of the Conference on Recent Advances in Particle Physics, New York Academy of Sciences (to be published); M. Jacob, CERN Report No. TH. 1639 (unpublished) (NAL-PUB-73/18-THY). Total cross-section data are from U. Amaldi *et al.* [Phys. Lett. **B44**, 112 (1973)] and S. R. Amendolia *et al.* [*ibid.* **B44**, 119 (1973)].

¹³K. G. Wilson, Acta Phys. Austr. **17**, 37 (1963).

¹⁴C. E. DeTar, Phys. Rev. D **3**, 128 (1971).

¹⁵A. H. Mueller, Phys. Rev. D **2**, 2963 (1970).

¹⁶J. Finkelstein and K. Kajantie, Nuovo Cimento **56A**, 659 (1968); R. C. Brower and J. H. Weis, Phys. Lett. **41B**, 631 (1972).

¹⁷A. H. Mueller, Phys. Rev. D **4**, 150 (1971).

- ¹⁸This has been shown in general by J. Koplik, Phys. Rev. D 7, 558 (1973).
- ¹⁹See the reviews by F. Zachariasen [Phys. Rep. 2C, 1 (1971); Caltech Report No. CALT-68-385, 1973 (unpublished)].
- ²⁰E. W. Anderson *et al.*, Phys. Rev. Lett. 25, 699 (1970).
- ²¹Rochester-Michigan collaboration, C. M. Bromberg *et al.*, University of Michigan Report No. UMBC 72-14 (unpublished).
- ²²This formula has a long history, which can be traced from Ref. 7.
- ²³Some confidence in the validity, or at least the utility, of this formula is developing as a result of a number of successful fits to data. See, for example, F. Sannes *et al.*, Phys. Rev. Lett. 30, 766 (1973); S. D. Ellis and A. I. Sanda, Phys. Rev. D 6, 1347 (1973); Phys. Lett. 41B, 87 (1972).
- ²⁴M. Bishari and J. Koplik [Phys. Lett. 44B, 175 (1973)] have observed that the J -plane singularities of this formula are a pole (from the first term in brackets) and a branch point (from the second term), which contribute with opposite sign. It is the coincidence of these singularities which causes the rising cross section discussed below.
- ²⁵D. M. Tow, Phys. Rev. D 7, 3535 (1973); R. N. Cahn, SLAC Report No. SLAC-PUB-1211 (unpublished). B. R. Webber [Nuovo Cimento Lett. 3, 424 (1972)] claims a similar but stronger result in which $B_0^i(t)$ is independent of t . This result follows from a strong version of the SRC hypothesis which is not supported by multi-peripheral or triple-Regge models.
- ²⁶M. Abramowitz and I. Stegun, *Handbook of Mathematical Functions* (Dover, New York, 1968), Secs. 6.5 and 26.4.
- ²⁷J. S. Ball and F. Zachariasen [Phys. Lett. 40B, 411 (1972)] obtain a similar result in the context of a self-consistent diffractive model. D. Silverman, P. Ting, and H. Yesian [Phys. Rev. D 5, 94 (1971)] carried out the same calculation in the context of different physical assumptions. They assumed P' dominance of σ_{aP} , so $\epsilon(t)$ was not small and the resulting distribution was geometrical rather than χ^2 .
- ²⁸R. Lipes, G. Zweig, and W. Robertson, Phys. Rev. Lett. 22, 433 (1969).
- ²⁹G. F. Chew and D. R. Snider, Phys. Lett. 31B, 75 (1970).
- ³⁰M. L. Goldberger, D. Silverman, and C.-I Tan, Phys. Rev. Lett. 26, 100 (1971).
- ³¹M. N. Misheloff, Phys. Rev. D 3, 1486 (1971).
- ³²M. L. Goldberger, C.-I Tan, and J. M. Wang, Phys. Rev. 184, 1920 (1969).
- ³³W. R. Frazer and C. H. Mehta, Phys. Rev. Lett. 23, 258 (1969).
- ³⁴The effects of secondary trajectories on rapidity distributions has been discussed by C.-I Tan, Phys. Rev. D 8, 935 (1973).